OSP 66896

REPORT DOCUMENTATION PAGE

AFRL-SR-AR-TR-02-

0219

1. AGENCY USE ONLY (Leave blank)	2. REPORT DATE	3. REPO... TYPE AND DATES COVERED
	6/4/2002	Final 3/1/1998 - 10/31/2001

4. TITLE AND SUBTITLE

Quantum Logic and Parallel Computing Using Spectral Holeburning Technologies

5. FUNDING NUMBERS

F49620-98-1-0313

6. AUTHOR(S)

Dr. Selim Shahriar, Prof. Shaoul Ezekiel, Prof. Seth Lloyd

7. PERFORMING ORGANIZATION NAME(S) AND ADDRESS(ES)

Research Laboratory of Electronics
Massachusetts Institute of Technology
77 Massachusetts Avenue
Cambridge, MA 02139

8. PERFORMING ORGANIZATION REPORT NUMBER

9. SPONSORING/MONITORING AGENCY NAME(S) AND ADDRESS(ES)

Air Force Office of Scientific Research
110 Duncan Avenue, Room B115
Bolling Air Force Base, DC 20332-8050

10. SPONSORING/MONITORING AGENCY REPORT NUMBER

2305/DS

11. SUPPLEMENTARY NOTES

The view, opinions and/or findings contained in this report are those of the author(s) and should not be construed as an official Department of the Army position, policy, or decision, unless so designated by other documentation.

12a. DISTRIBUTION/AVAILABILITY STATEMENT

Approved for public release; distribution unlimited.

12b. DISTRIBUTION CODE

13. ABSTRACT (

The objective of this project was to investigate the use of spectral holeburning technologies for quantum logic and parallel computing. To this end, we have made substantial progress on both experimental and theoretical fronts. In NV-diamond, we have demonstrated the alignment of spins, which can then be used as quantum bits for a quantum computer. We have performed high resolution imaging of color centers in NV-diamond, as a key step towards isolating and detecting individual quantum bits. We have also developed a detailed model for cavity induced coupling of qubits in this system. Furthermore, we have developed a concrete design for producing a photonic band gap based cavity directly in a diamond substrate. Such a cavity will have the requisite combination of high finesse and low loss necessary for photon-mediated coupling of qubits, which is not possible using bulk mirror cavities because of high surface reflection losses from an embedded crystal. We have also developed a novel model for cavity-induced coupling via the atom-cavity-dark-state, a process that is robust against atomic as well cavity decay. Finally, we have identified a mechanism for direct dipole-dipole coupling of the qubits as well. This scheme is particularly well suited for creating in parallel many quantum computers, each containing a small number of coupled qubits. Dubbed Type II Quantum Computing, this architecture is expected to outperform the best classical computers in specialized tasks such as modeling turbulence through the cellular automaton based lattice gas dynamics. In Pr:YSO, we have demonstrated a slowing (45 m/sec) and high-fidelity storage and recall of light pulses. This scheme is expected to enable the realization of a near-perfect quantum memory for single-photons, storing and recalling it with near 100% fidelity. A variation of the same process may be useful in generating a macroscopic entanglement of the type recently proposed for atomic vapor cells. Work carried out under this project has resulted in the publication of many conference papers, several manuscripts in review, and seven published/accepted articles in refereed journals , two of which are in the Physical Review Letters, as well as popular articles in journals such as The New Scientist and The Business Week.

14. SUBJECT TI

AGES

16. PRICE CODE

17. SECURITY CLASSIFICATION OF REPORT	18. SECURITY CLASSIFICATION OF THIS PAGE	19. SECURITY CLASSIFICATION OF ABSTRACT	20. LIMITATION OF ABSTRACT
UNCLASSIFIED	UNCLASSIFIED	UNCLASSIFIED	UL

Quantum Logic and Parallel Computing Using Spectral Holeburning Technologies

Grant#: F49620-98-1-0313
OSP#: 6689600

FINAL REPORT

Co-Principal Investigators:
Dr. Selim Shahriar, Prof. Shaoul Ezekiel, Prof. Seth Lloyd

ABSTRACT

The objective of this project was to investigate the use of spectral holeburning technologies for quantum logic and parallel computing. To this end, we have made substantial progress on both experimental and theoretical fronts. In NV-diamond, we have demonstrated the alignment of spins, which can then be used as quantum bits for a quantum computer. We have performed high resolution imaging of color centers in NV-diamond, as a key step towards isolating and detecting individual quantum bits. We have also developed a detailed model for cavity induced coupling of qubits in this system. Furthermore, we have developed a concrete design for producing a photonic band gap based cavity directly in a diamond substrate. Such a cavity will have the requisite combination of high finesse and low loss necessary for photon-mediated coupling of qubits, which is not possible using bulk mirror cavities because of high surface reflection losses from an embedded crystal. We have also developed a novel model for cavity-induced coupling via the atom-cavity-dark-state, a process that is robust against atomic as well cavity decay. Finally, we have identified a mechanism for direct dipole-dipole coupling of the qubits as well. This scheme is particularly well suited for creating in parallel many quantum computers, each containing a small number of coupled qubits. Dubbed Type II Quantum Computing, this architecture is expected to outperform the best classical computers in specialized tasks such as modeling turbulence through the cellular automaton based lattice gas dynamics. In Pr:YSO, we have demonstrated a slowing (45 m/sec) and high-fidelity storage and recall of light pulses. This scheme is expected to enable the realization of a near-perfect quantum memory for single-photons, storing and recalling it with near 100% fidelity. A variation of the same process may be useful in generating a macroscopic entanglement of the type recently proposed for atomic vapor cells. Work carried out under this project has resulted in the publication of many conference papers, several manuscripts in review, and seven published/accepted articles in refereed journals , two of which are in the Physical Review Letters, as well as popular articles in journals such as The New Scientist and The Business Week.

REPORT DOCUMENTATION

1. LIST OF PUBLICATIONS AND MANUSCRIPTS:

Published or Accepted for Publications:

1. "Cavity Dark State for Quantum Computing," M.S. Shahriar, J. Bowers, S. Lloyd, P.R. Hemmer, and P.S. Bhatia, *Opt. Commun.* **195**, 5-6 (2001).
2 . "Raman Excited Spin Coherence in NV-Diamond," P.R. Hemmer, A.V. Turukhin, M.S. Shahriar, and J.A. Musser, *Opt. Letts.* **26**, 6 (2001).
3. "Demonstration of Injection Locking a Diode Laser Using a Filtered Electro-Optic Modulator Sideband," M.S. Shahriar, A.V. Turukhin, T. Liptay, Y. Tan, and P.R. Hemmer, *Opt. Commun.* **184**, 5-6 (2000).
4. "Long Distance, Unconditional Teleportation of Atomic States via Complete Bell State Measurements," S. Lloyd, M.S. Shahriar, J.H. Shapiro, and P.R. Hemmer, *Phys. Rev. Lett.* **87**, 167903 (2001).
5. "Observation of Ultraslow and Stored Light Pulses in a Solid," A. V. Turukhin, V.S. Sudarshanam, M.S. Shahriar, J.A. Musser, B.S. Ham, and P.R. Hemmer, *Phys. Rev. Lett.* **88**, 023602 (2002).
6. "Solid-state Quantum Computing using Spectral Holes," M.S. Shahriar, P.R. Hemmer, P.S. Bhatia, S. Lloyd, and A.E. Craig, to appear in *Phys. Rev. A.*
7. "Frequency Stabilization of an Extended Cavity Semiconductor Laser for Chirped Cooling," J.A. Morzinsky, P.S. Bhatia, and M.S. Shahriar, to appear in *Review of Scientific Instruments.*

Papers in Review:
1. "Phase-Locking of Remote Clocks using Quantum Entanglement," M.S. Shahriar, submitted to *Phys. Rev. Letts. (http://xxx.lanl.gov/pdf/quant-ph/0010007).*
2. "Determination of the Phase of an Electromagnetic Field via Incoherent Detection of Fluorescence," M.S. Shahriar, P. Pradhan, and J. Morzinsky, submitted to *Phys. Rev. Letts.*

Conference Presentations:

1. "Quantum Computation via Spectral Holeburning in a Crystal," M.S. Shahriar, J. Bowers, S. Lloyd, A. Craig and P.R. Hemmer, *IX Conference on Laser Optics*, 1998, St. Petersburg, Russia **(invited).**
2. "Quantum Computation via Coherent Population Trapping in an Inhomogeneously Broadened Crystal," M.S. Shahriar, J. Bowers, S. Lloyd, A. Craig and P.R. Hemmer, *the 4th International Conference on Quantum Communication, Measurement, and Computing,* 1998, Evanston, IL.
3. "Quantum Computing via Cavity Induced Coupling of Spectrally Selective Bands of Particles in a Solid," M.S. Shahriar, J. Bowers, S. Lloyd, A. Craig and P.R. Hemmer, *the OSA Topical Meeting on Optics in Computing*, 1999, Snowmass, CO. **(invited).**

4. P.R. Hemmer, M.S. Shahriar, and A. Turukhin, "Raman excited spin coherences for high-temperature spectral hole-burning memories" *Proceedings of the Conference on Lasers and Electro-Optics*, San Francisco, CA, 2000.
5. "Quantum Computing in Diamond," . M.S. Shahriar, A.V. Turukhin, P.R. Hemmer, and S. Lloyd, proceedings of the *International Conference on Experimental Implementation of Quantum Computing*, 16-19 January, 2000, Sydney, Australia **(Invited).**
6. "Type II Quantum Computing in Spectrally Selective Solids," M.S. Shahriar, S. Lloyd, and P.R. Hemmer, *Proceedings of the Quantum Computing for Physical Modeling* conference, Oct. 18-19, 2000, North Falmouth, MA **(Invited).**
7. "Raman Excited Spin Alignment in NV Diamond," A. Turukhin, M.S. Shahriar, P.R. Hemmer, and J.A. Musser, *Proceedings of Optical Society of America Annual Meeting*, Providence, RI, October 2000 **(postdeadline)**
8. "Raman Excited Spin Coherence in NV Diamond," P.R. Hemmer, A. Turukhin, M.S. Shahriar, and J.A. Musser, *proceedings of the International Quantum Electronics Conference*, Baltimore, MD, May 2001.
9. "Observation of Ultraslow Group Velocity of Light in a Pr:YSO crystal," V.S. Sudarshanam, M.S. Shahriar, and P.R. Hemmer, *31st Winter Colloquium in Quantum Electronics*, Snowbird, Utah (Jan 2001).
10. "First Observation of Ultraslow Group Velocity of Light in a Solid," A. Turukhin, V.S. Sudarshanam, M.S. Shahriar, J.A. Musser, and P.R. Hemmer, proceedings of the *International Quantum Electronics Conference*, Baltimore, MD, May 2001.
11. "Spin Mediated Slowing and Stoppage of Light in a Solid," A.V. Turukhin, M.S. Shahriar, J.A. Musser, and P.R. Hemmer, *proceedings of Spintech 1*, Maui, Hawaii, May 2001.
12. "First Observation of Ultraslow Group Velocity of Light in a Solid," A. Turukhin, V.S. Sudarshanam, M.S. Shahriar, J.A. Musser, and P.R. Hemmer, *proceedings of the SPIE Conference,* San Diego, CA August 2001 **(Invited)**.
13. "Raman Excited Spin Coherence in NV Diamond," P.R. Hemmer, A. Turukhin, M.S. Shahriar, and J.A. Musser, *proceedings of the SPIE Conference,* San Diego, CA August 2001 **(Invited)**.
14. "Bloch-Siegert oscillation for detection and quantum teleportation of the phase of an oscillating field," M.S. Shahriar, *proceedings of the Conference on Quantum Optics 8*, Rochester, NY, July 2001.
15. "Long-distance, unconditional teleportation of atomic states via complete measurement of all Bell-states," M.S. Shahriar, S. Lloyd, J.H. Shapiro, and P.R. Hemmer, *proceedings of the International Conference on Quantum Information,* Rochester, NY, July 2001.
16. "Quantum Computing using NV-Diamond," M.S. Shahriar, to be presented at *the Progress in Quantum Electronics conference*, Snowbird, UT, Jan. 2002 **(Invited).**

2. REPORT OF INVENTIONS

Experimental:

- *Demonstrated technique for near-perfect spin alignment in NV-diamond for applications to quantum computing*
- *Demonstrated technique for producing ultraslow group velocity of light in a solid*
- *Demonstrated technique for high-fidelity storage and recall of photons in a solid*
- *Demonstrated technique for injection locking of diode lasers Using cavity-filtered EOM sideband*
- *Demonstrated technique for reference locked scanning of diode lasers*
- *Photonic band-gap cavity design in NV-Diamond for coupling quantum bits*

Theoretical:

- *Developed a method for creating entanglement between two qubits using transfer of quantum coherence via non-degenerate sub-levels, a process essential for realizing a quantum computer in NV-diamond*
- *Developed a method for realizing controlled-NOT gates in NV-diamond via direct dipole-dipole coupling between qubits that are spatially adjacent, and can be tuned to become spectrally adjacent using time-dependent magnetic fields.*
- *Developed a method for coupling quantum bits robustly using cavity dark states*
- *Developed a detailed model for quantum computing using NV-diamond*

3. SCIENTIFIC PROGRESS AND ACCOMPLISHMENTS

The objective of this project was to investigate the use of spectral holeburning technologies for quantum logic and parallel computing. To this end, we have made substantial progress on both experimental and theoretical fronts. In NV-diamond, we have demonstrated the alignment of spins, which can then be used as quantum bits for a quantum computer. We have performed high resolution imaging of color centers in NV-diamond, as a key step towards isolating and detecting individual quantum bits. We have also developed a detailed model for cavity induced coupling of qubits in this system. Furthermore, we have developed a concrete design for producing a photonic band gap based cavity directly in a diamond substrate. Such a cavity will have the requisite combination of high finesse and low loss necessary for photon-mediated coupling of qubits, which is not possible using bulk mirror cavities because of high surface reflection losses from an embedded crystal. We have also developed a novel model for cavity-induced coupling via the atom-cavity-dark-state, a process that is robust against atomic as well cavity decay. Finally, we have identified a mechanism for direct dipole-dipole coupling of the qubits as well. This scheme is particularly well suited for creating in parallel many quantum computers, each containing a small number of coupled qubits. Dubbed Type II Quantum Computing, this architecture is expected to outperform the best classical computers in specialized tasks such as modeling turbulence through the cellular In Pr:YSO, we have demonstrated a slowing (45 m/sec) and high-fidelity storage and recall of light pulses. This scheme is expected to enable the realization of a near-perfect quantum memory for single-photons, storing and recalling it with near 100% fidelity. A variation of the same process may be useful in generating a macroscopic entanglement of the type recently proposed for atomic vapor cells.

3.1 Explicit Model for Quantum Computing in a Spectral Holeburning Solid

We have developed an explicit model for producing entanglement between qubits that are spectral neighbors. The model also includes a pair of shelving levels in each atom for storing the qubit during inactive periods, providing isolation while neighbors interact. This model is illustrated in figures 1, 2 and 3.

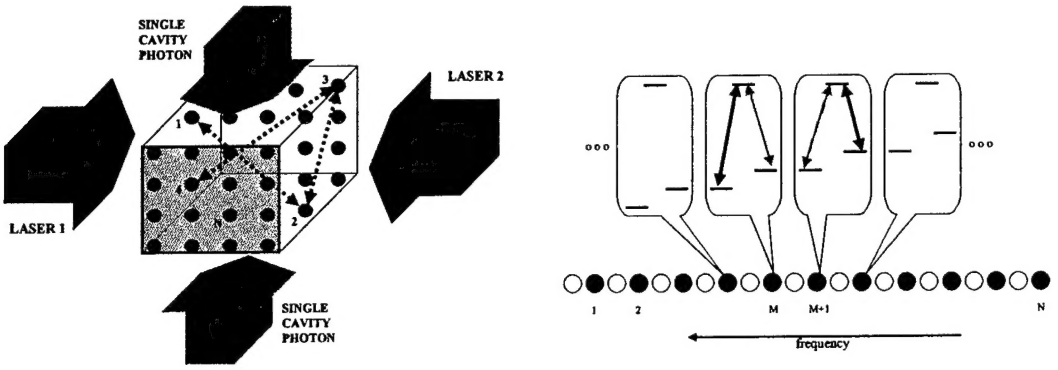

Figure 1: *Schematic Illustration of coupling inhomogeneously broadened atoms using spectral selectivity. The top figure shows a small volume of a crystal, selected by the intersection of the cavity mode and the control laser beams. The bottom figure shows how the atoms can be indexed in terms of their frequency response. Spectrally adjacent atoms, with a frequency difference matching the ground state splitting, can be coupled selectively by tuning the cavity and the coupling lasers. Atom M can be addressed spectrally via the red transition, atom M+1 can be addressed via the purple transition, and the two are coupled to the cavity via the blue transition.*

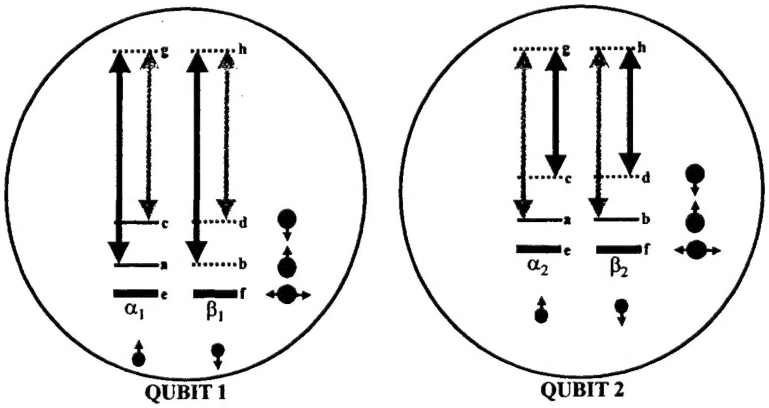

Figure 2: *Relevant energy levels and transitions required of two spectrally adjacent atoms in this scheme. In each atom, the six low-lying levels can be thought of as corresponding to the spin states of two pseudo-particles: a spin 1 particle (A: red) and a spin ½ particle (B: blue). In the quiescent state, the qubit in each atoms is represented by the spin-up (0=e) and spin-down (1=f) states of B, with A in the spin-horizontal state, containing no information. Whenever it is necessary to perform a gate operation*

between two neighboring qubits, the qubit in atom 1 ($\alpha_1|e\rangle+\beta_1|f\rangle$) is transferred to the spin-up and -down states of A_1, with B_1 in the spin-up state ($\alpha_1|a\rangle+\beta_1|c\rangle$). This pattern is alternated in the subsequent atoms in the chain. The qubit in atom 2 ($\alpha_2|e\rangle+\beta_2|f\rangle$) is transferred to the spin-up and -down states of B_1, with A_1 in the spin-up state ($\alpha_2|a\rangle+\beta_2|b\rangle$). As shown by Pellizari et al.[4], using a sequence of pulses from the red (resonant with atom 2) and orange (resonant with atom 1) lasers, the quantum states are exchanged between A_1 and A_2, via the "quantum wire" provided by the blue cavity photon, which has a common resonance with both atoms. Conceptually, this can be thought of as a two-step process. First, the orange laser transfers the state of A_1 to the cavity, producing a superposition of 0 and 1 photons ($\alpha_1|1\rangle+\beta_1|0\rangle$). The red laser then transfers this state to A_2 ($\alpha_1|\downarrow\rangle+\beta_1|\uparrow\rangle$). All four bits of information are now in atom 2; as such, any desired gate operation (see fig. 4) can be achieved by a pulse coupling any two of the states (a,b,c,d), using a two-photon transition. A_2 is now exchanged with A_1 by using a reverse sequence of the red and orange lasers. Finally, the state of each atom is transferred to the levels e and f. These storage levels (with the e-a frequency different from the a-c frequency) are essential in this scheme in order to make sure that the populated levels of the other, quiescent neighboring qubits remain unaffected by these gate operations.

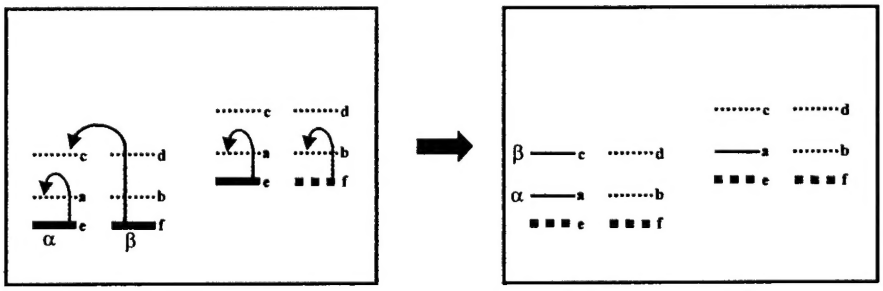

[A]

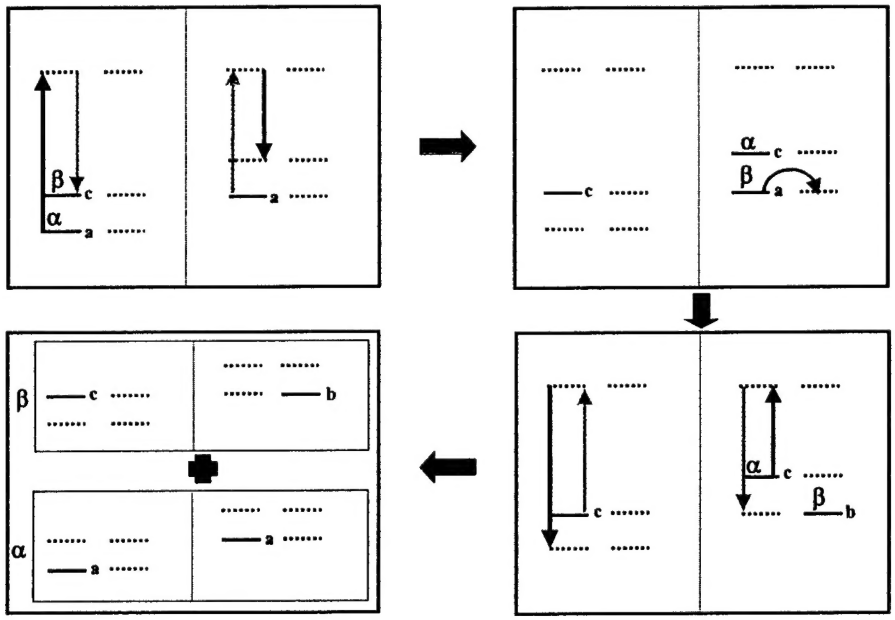

[B]

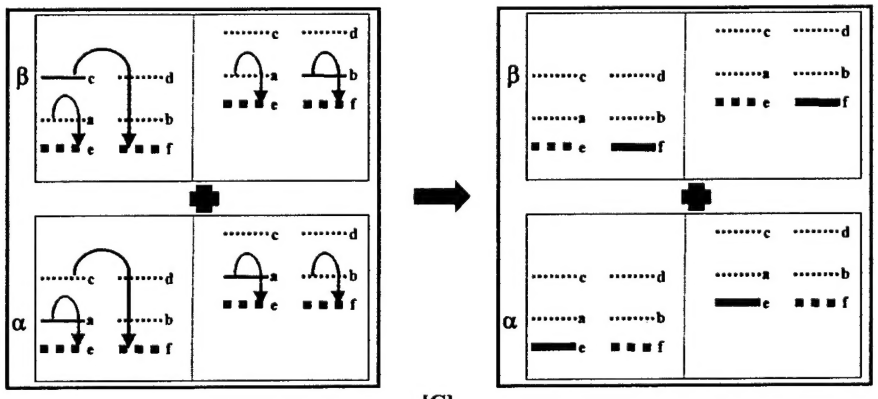

[C]

Figure 3: *Illustration of the steps necessary to produce entanglement, starting from a joint state* $(\alpha|0\rangle+\beta|1\rangle)\otimes|0\rangle$. *(a) The state of each qubit is retrieved from the storage levels, using off-resonance Raman* π *pulses, producing* $(\alpha|a\rangle+\beta|c\rangle)\otimes|a\rangle$; *the additional levels in the excited states of both Pr:YSO and NV-diamond allow for these two-photon transitions. Either polarization selection rules or an external magnetic field can be used to provide the selectivity of the desired transition (b) A pulse sequence of the orange and red lasers exchanges, via the common cavity photon, the states of* A_1 *and* A_2 *(see fig. 2), producing* $|c\rangle\otimes(\alpha|c\rangle+\beta|a\rangle)$. *Another off-resonance Raman* π *pulse is used to transfer a to b, producing* $|c\rangle\otimes(\alpha|c\rangle+\beta|b\rangle)$; *this is a controlled-NOT operation that entangles* A_2 *and* B_2. *A reverse pulse sequence of orange and red lasers exchanges back the states of* A_1 *and* A_2, *producing* $(\alpha(|aa\rangle+\beta|cb\rangle)$, *which represents an entangled state of the two atoms. (c) The state of each qubit is now returned to the storage levels, producing the*

final state of ($\alpha|00\rangle+\beta|11\rangle$), corresponding to a controlled-NOT operation between the two qubits.

3.2 Robust coupling of quantum bits via cavity dark states

We have also developed a new method of inter-atomic coherence transfer; termed adiabatic evolution via a cavity dark state, this eliminates the effect of cavity decay. This method is illustrated schematically in figures 1 and 2. Furthermore, we have constructed a cavity structure which enables the use of multiple spatial modes for the coherence transfer, yielding a strong vacuum rabi frequency (~MHz) and a narrow linewidth (~kHz).

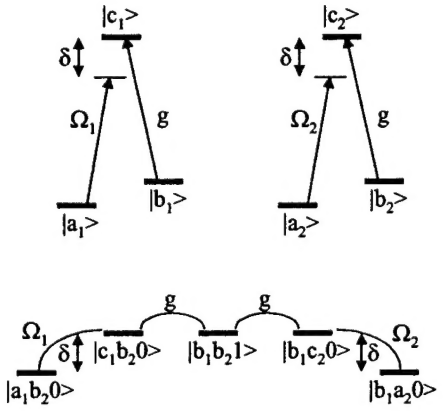

Figure 1: *Illustration of the excitation scheme needed to implement a cavity dark state. As shown in the top diagram, the classical laser beams are detuned, while the cavity is kept on resonance. The bottom diagram shows the same situation in the rotating wave frame. The state $|b_1b_20\rangle$ (not shown) is still the trivial dark state.*

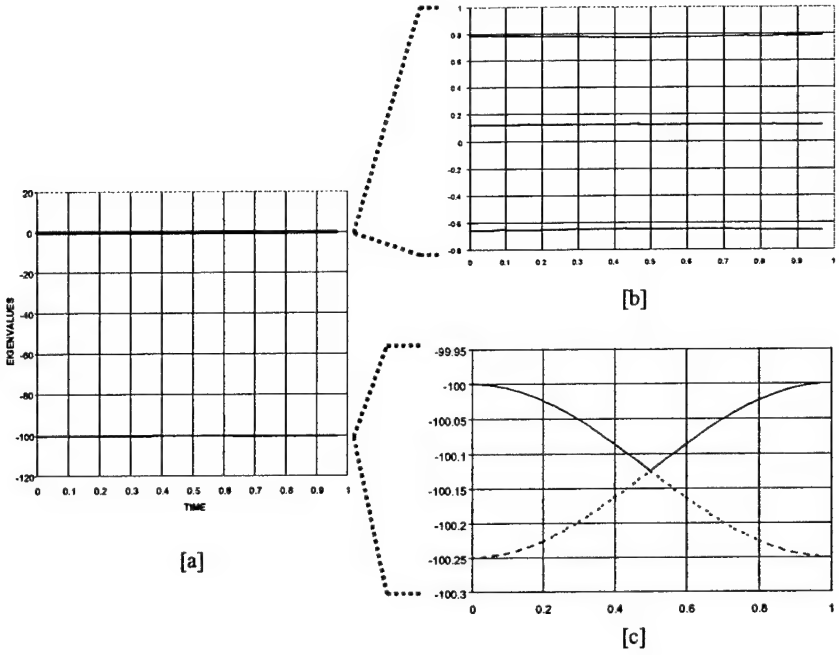

Figure 2: *Illustration of the dressed states corresponding to the system of two atoms coupled to the cavity, as functions of the interaction interval during which both laser pulses are present. (a) All five dressed states on the same scale (b) Expanded view of the dressed states that evolve adiabatically from/to the states |1>, |2> and |3> (c) Expanded view of the dressed states that evolve adiabatically from/to the states |4> and |5>.*

3.3 Raman Excited Spin Alignment in NV-Diamond

Previously, we have reported on the observation of near perfect alignment of spins in NV-diamond, which can then be used as quantum bits (qubits) for a quantum computer (QC). We have continued studying this process in order to determine the optimum conditions for manipulating quantum bits via this process. In particular, we have studied the dependence of the spin alignment on magnetic field, intensity of the Raman fields, and the strength of the repump laser.

Recalling briefly, our approach is based on the two-photon excitation of resonant transitions modified by a dipole-dipole interaction and presented in detail elsewhere. Our existing sample 30 ppm NV-diamond was evaluated to be very promising for experimental realization of the proposed approach. In particular, optical transition at 637 nm has an inhomogeneous broadening of 750 GHz, and inhomogeneous width of 50 MHz.

The experimental setup used in the N-V diamond studies is shown in Figure 1. Here, a Raman enhanced non-degenerate four-wave mixing (NDFWM) technique is used to achieve a high signal to noise ratio, in analogy to experimental techniques used previously to study Pr:YSO . In this scheme, coupling (C) and probe (P) field are used to write a grating in the ground state spin coherence via the resonance Raman interaction.

This grating is read with a read beam (R) to produce a signal or diffracted beam (D). To further enhance signal to noise, a heterodyne detection scheme is used as shown in Figure 1(b). All dye laser beams are derived from a single dye laser output using acousto-optic frequency shifters. This greatly relaxes dye laser frequency stability requirements since the resonant Raman interaction is insensitive to correlated laser jitter. An additional beam from the argon laser (A) is also directed into the sample to serve as a repump. Without this repump beam, the N-V center would exhibit long-lived spectral hole-burning and no cw signal would be seen after a short time. The Raman transition frequency (~120 MHz) is determined by the spacing between the S=0 and S=-1 ground state spin sublevels. This spacing is controlled by applying a magnetic field of about 1 kGauss along the crystal (111) direction. At this field strength, the S=0 and S=-1 ground sublevels (for N-V centers aligned along (111)) are near an anti-crossing. These conditions are chosen to enhance Raman transition strength by compensating for the small spin-orbit coupling in diamond with a partial mixing the spin sublevels.

The observed NDFWM signal is shown in Figure 2 as a function of Raman detuning. For convenience, the Raman detuning is adjusted by tuning the spacing between the S=0 and S=-1 sublevels using the applied magnetic field. As shown, the Raman linewidth is about 20 MHz, which is comparable to the 15 MHz inhomogeneous width of the ground state spin transition. This width is significantly smaller than the homogeneous width (>>25 MHz) of the optical transition and laser jitter (~100 MHz), and is taken as evidence of the Raman process. The asymmetry in the lineshape is due to interference with the (much broader) NDFWM signal at the anti-crossing. To eliminate this interference and to improve quality of the NDFWM signal, scanning of probe beam frequency is required. This was achieved by introducing electro-mechanical galvos. Compensating of angular displacement of coupling, probe, and reading beams, galvos allow scanning frequency of all beams. To further expand capability of the experimental setup, RF drivers for AOMs were configured to scan difference frequency between coupling and probe beam. A representative NDFWM signal obtained with modified setup is shown in Figure 3 as a function of frequency difference between coupling and probe beam. The value of the magnetic field was chosen about 1 kGauss and maintained constant.

Large optical matrix elements are required to maximize the number of gate operations per decoherence time. To evaluate matrix elements of our system, we investigated NDFWM diffraction amplitude as a function of laser intensity. The results are shown in Figure 4 for different laser intensities of coupling and probe beams. Intensity of the read beam was 25 W/cm^2, and intensity of the repump beam was around 10 W/cm^2. Saturation intensities were found to be 5 W/cm^2 and 3 W/cm^2 for coupling and probe transition respectively. Relatively high values of saturation intensities might be explained high optical density of this particular sample. Using obtained values of optical matrix elements, we can expect 100-1000 logic gate operations per spin decoherence time.

It is interesting to note that laser intensity has a great influence not only on amplitude of the NDFWM signal, but also on symmetry of lineshape. Figure 5 illustrates observed this dramatic change in lineshape.

Trying to optimize experimental conditions for observation of NDFWM signal, we studied NDFWM signal lineshape as a function of applied magnetic field. The

experimental results are show in Figure 7. Sharp reduction in amplitude of the observed NDFWM signal far from central frequency most likely can be explained by limited bandwidth of the AOM used to scan the frequency of the probe beam. Further investigation of the obtained dependencies with proper renormalization of the signal is planed for the future.

Finally, Raman induced transparency of the probe field (P) has also been observed. Applying coupling laser power about 13 W/cm^2 , absorption suppression of the probe beam (1.3 W/cm^2) was evaluated to be about 4% (that corresponds change in transmission to be about 2.5%). Experimental traces are presented in Figure 8.

As a first step in investigation of spin echo in NV-diamond, we studied optical pumping effect on population of ground state. Regular NMR signal was detected at 430 MHz with applied magnetic field of 920 Gauss. RF power was modulated by square wave with frequency 50 Hz. Considering long lifetime of the metastable ground state, fall time of the observed pulses was strongly depended on efficiency of optical pumping. Experimental decay curve revealed two components: one weak component had constant fall time of about 5 ms, and the second stronger component had much shorter fall time, heavily depended on laser intensity. Therefore, weak component was attributed to unknown background signal, and the strong component was attributed to studied optical pumping effect. Experimental decay curves and corresponding fitting curves are shown in Figure 9.

Preliminary analysis of the NV-diamond showed a good potential of this material for experimental realization of solid state quantum computing based on dipole-dipole coupling. It was estimated that existing sample can provide as many as 900 coupled qubits per laser spot for quantum computing in spectrally selective solids. Dark raman resonances are observed and studied. Effects of laser power and magnetic field on Raman enhanced non-degenerate four-wave mixing signal are discussed. Optical matrix elements are found to be sufficient to allow 100-1000 logic gates operation per spin decoherence time. preliminary results on spin echo in NV-diamond are presented.

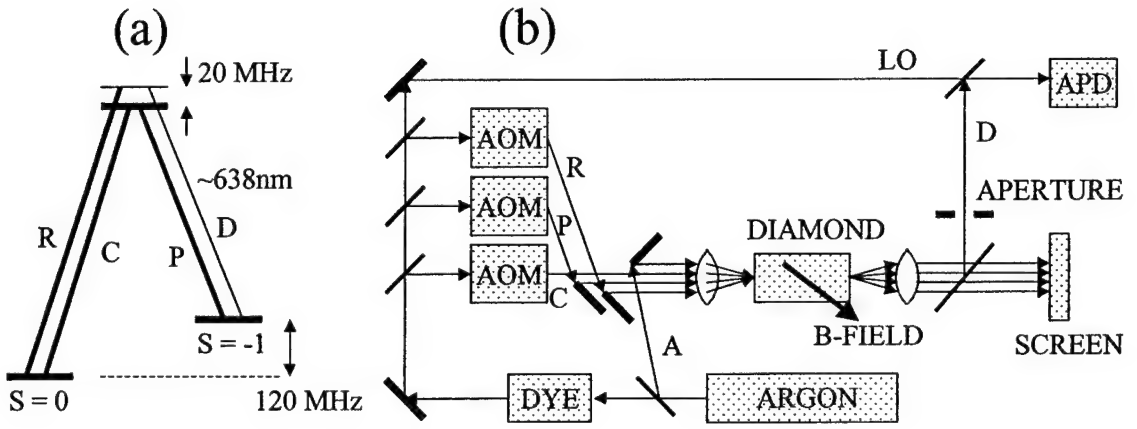

Figure 1. Experimental setup for observation of Raman excited spin coherences in N-V diamond. (a) Level diagram near anti-crossing. (b) Optical table setup.

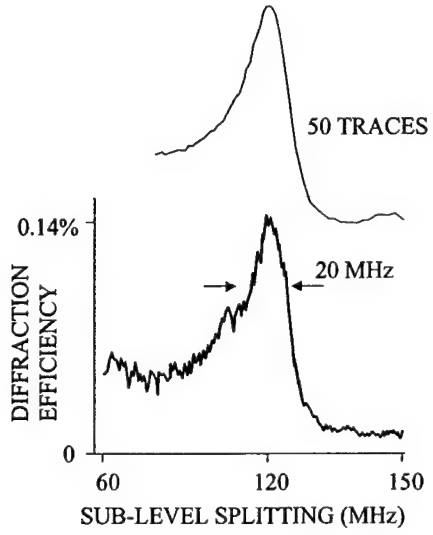

Figure 2. Raman enhanced non-degenerate four-wave mixing signal vs. magnetic field induced splitting of S=0,-1 states.

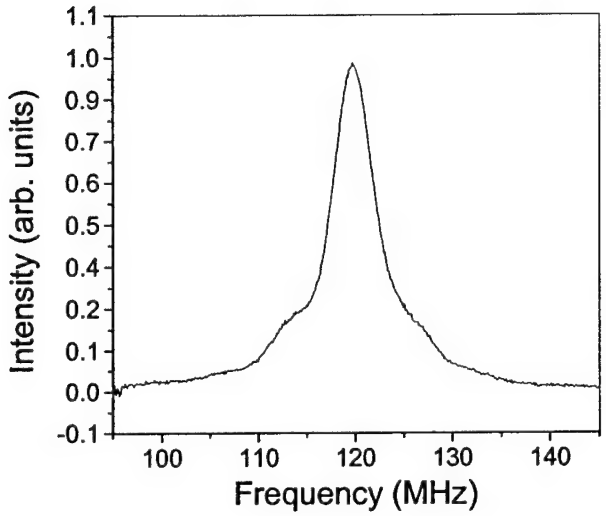

Figure 3. Raman enhanced non-degenerate four-wave mixing signal vs. frequency difference between coupling and probe beam.

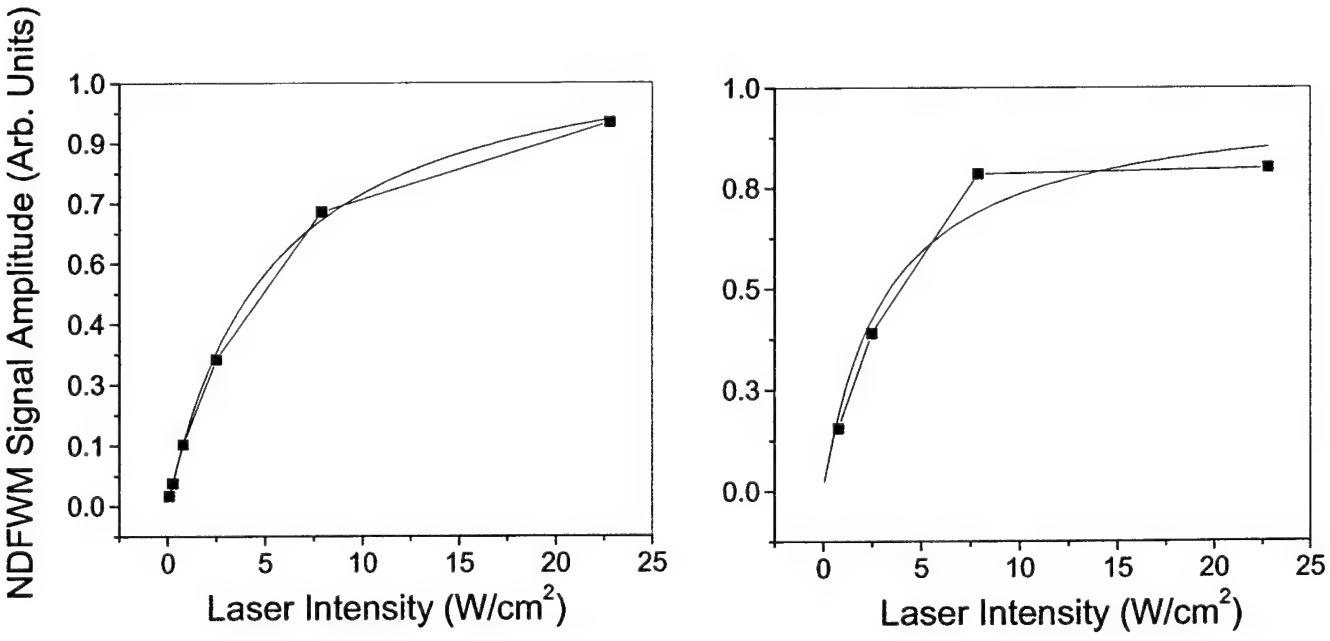

Figure 4. Amplitude of Raman enhanced non-degenerate four-wave mixing signal vs. laser intensity of coupling (left chart) and probe (righ chart) beams.

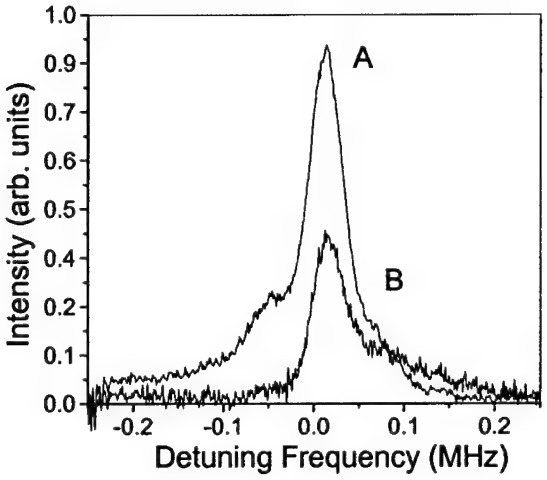

Figure 6. Observed raman enhanced non-degenerate four-wave mixing signal lineshape with applied full laser power (trace A) and 1/3 of full laser power (trace B).

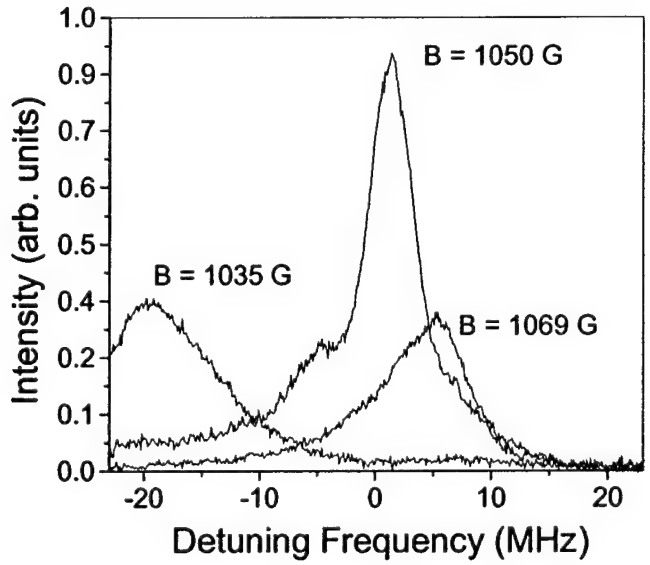

Figure 7. Raman enhanced non-degenerate four-wave mixing signal vs. magnetic field strength.

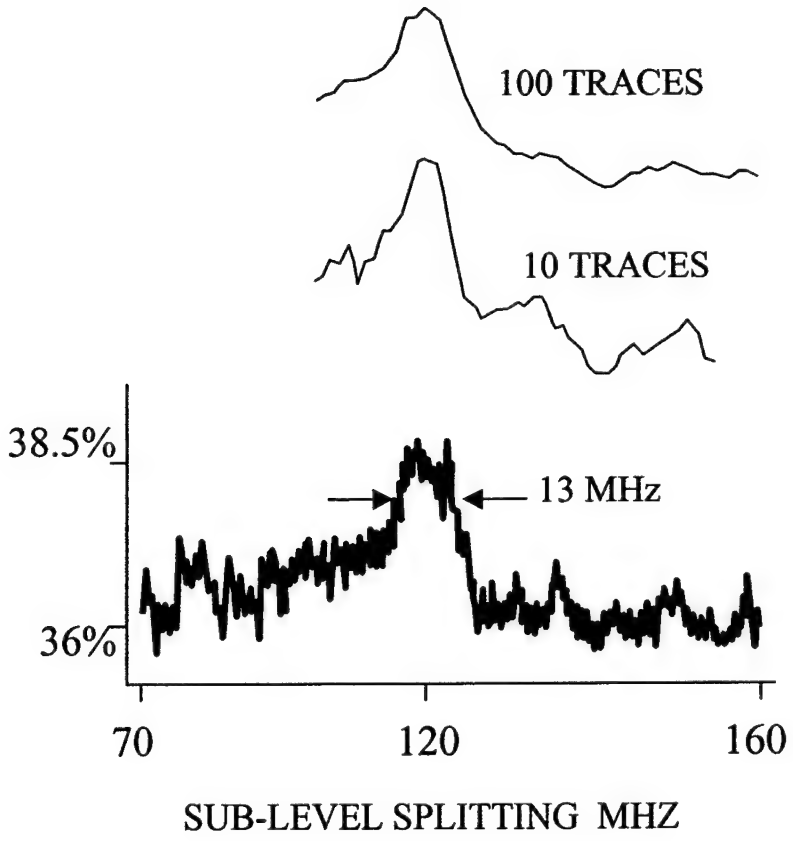

Figure 8. Absorption suppression in NV-diamond. Observed change in probe beam transmission is shown.

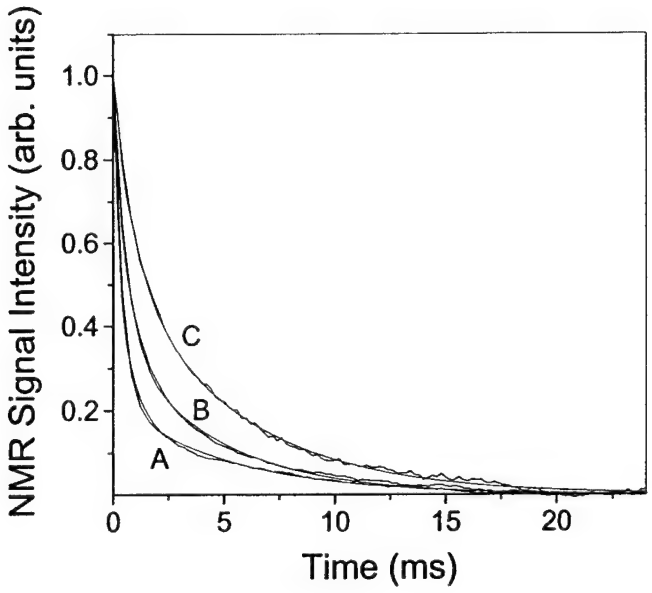

Figure 9. Ground state optical pumping after RF-pulse in NV-diamond. Optical pumping times of 0.40 ms, 0.58 ms, and 0.94 ms were found for laser powers of 96 mW/cm^2 , 48 mW/cm^2 , and 24.

3.4 Entanglement via Cavity-Induced Coherence Transfer using Non-degenerate Zeeman Sublevels:

As described in the previous report, we have a concrete model for coupling spectrally adjacent qubits in a spectral-hole-burning medium such as NV-diamond. For convenience, the essential element of this scheme is summarized in figure 1, which shows the relevant energy levels and transitions required of two spectrally adjacent atoms in this scheme. In each atom, the six low-lying levels can be thought of as corresponding to the spin states of two pseudo-particles: a spin 1 particle (A) and a spin ½ particle (B). In the quiescent state, the qubit in each atoms is represented by the spin-up (0=e) and spin-down (1=f) states of B, with A in the spin-horizontal state, containing no information. Whenever it is necessary to perform a gate operation between two neighboring qubits, the qubit in atom 1 ($\alpha_1|e\rangle+\beta_1|f\rangle$) is transferred to the spin-up and -down states of A_1, with B_1 in the spin-up state ($\alpha_1|a\rangle+\beta_1|c\rangle$). This pattern is alternated in the subsequent atoms in the chain. The qubit in atom 2 ($\alpha_2|e\rangle+\beta_2|f\rangle$) is transferred to the spin-up and -down states of B_2, with A_2 in the spin-up state ($\alpha_2|a\rangle+\beta_2|b\rangle$). Using a sequence of pulses from the green and red lasers, the quantum states are exchanged between A_1 and A_2, via the "quantum wire" provided by the blue cavity photon. Conceptually, this can be thought of as a two-step process. First, the red laser transfers

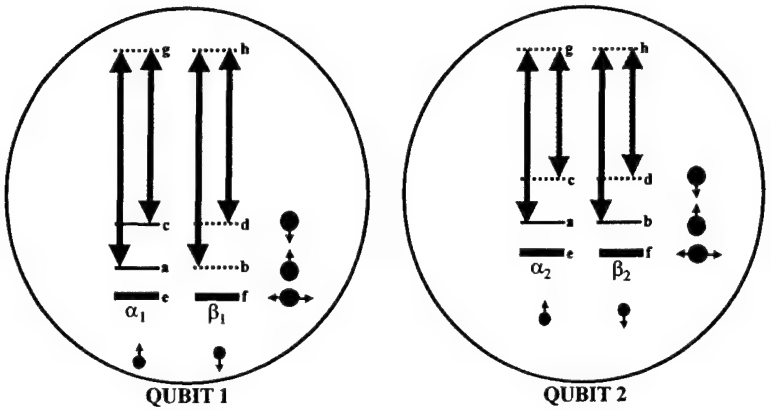

Figure 1: *Schematic illustration of the energy level structure required for coupling spectrally adjacent qubits in a spectral-hole-burning medium. See text for detail.*

the state of A_1 to the cavity, producing a superposition of 0 and 1 photons ($\alpha_1|1>+\beta_1|0>$). The green laser then transfers this state to A_2 ($\alpha_1|\downarrow>+\beta_1|\uparrow>$). All four bits of information are now in atom 2; as such, any desired gate operation can be achieved by a

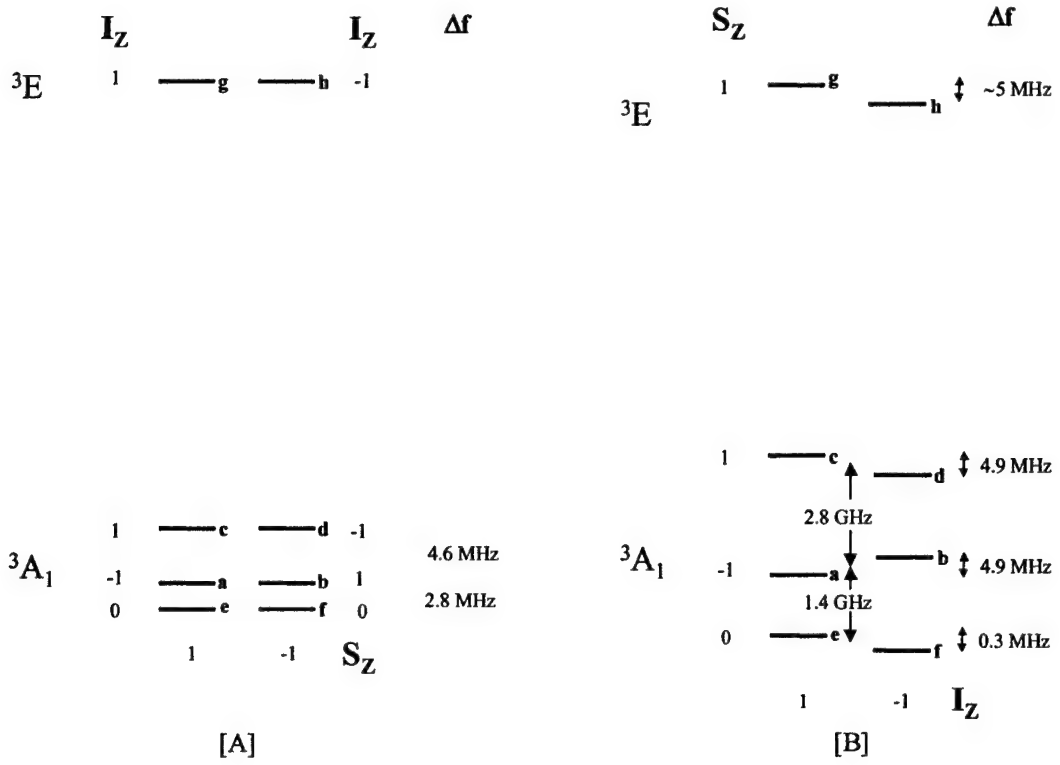

Figure 2. *Relevant subset of energy levels of the candidate material: N-V color centers in diamond. The $^3A_1$ to ^3E transition is excited at 637.8 nm, with a homogeneous linewidth of 5 MHz and an inhomogeneous linewidth of 1 THz at liquid helium temperature. The energy sublevels correspond to the spin orientations of the two uncoupled electrons (S) and the nucleus (I) of the substitutional nitrogen atom. [A] The levels at zero magnetic field. The inter-qubit frequency spacing in this case is 4.6 MHz, corresponding to more than 10^5 qubits per spot. [B] The levels at a magnetic field of 500 Gauss, including nuclear Zeeman splitting of 300 Hz/Gauss. The inter-qubit spacing in this case is 2.8 GHz, corresponding to about 300 qubits per spot.*

pulse coupling any two of the states (a,b,c,d), using a two-photon transition. A_2 is now exchanged with A_1 by using a reverse sequence of the red and green lasers. Finally, the

state of each atom is transferred to the levels e and f. These storage levels are needed to ensure that the neighboring qubits remain unaffected by these gate operations.

We have identified the corresponding energy levels in NV-diamond, as shown in figure 8a, corresponding to zero external magnetic field. However, under this condition (i.e., zero magnetic field), the spin-orbit coupling necessary for Raman transition is virtually non-existent. The spin-orbit coupling can be enhanced strongly by applying a magnetic field of about 1 kilo Gauss, thereby mixing the levels of figure 2a. The resulting energy levels are shown in figure 2b. As can be seen, the pair-wise degeneracy of levels --- as required from figure 1 --- is no longer present in figure 8b.

We have developed a scheme whereby it is possible to realize the coupling even in the absence of the pair-wise level degeneracy. Briefly, one has to use two lasers frequencies simultaneously for each of the external control beams shown in figure 1. In order for the protocol to work under this condition, the constraint is that each of these two frequencies should excite one and only one of the optical transitions. This condition can be satisfied easily for the energy levels of NV-diamond shown in figure 2b.

3.5 Controlled-NOT using Direct Dipole-Dipole coupling in NV-Diamond:

If the effective density of color centers is high, then one can make use of the direct dipole-dipole coupling between color centers. The basic dipole-dipole coupling scheme has been developed by affiliate members of our project. Briefly, two atoms (or color centers) must be identified that are spatially separated by a distance of less than $\lambda/10$ where λ is the optical wavelength of a convenient Raman transition. The optical transitions of the two atoms must also be close enough that components of the Raman transitions on neighboring atoms can be tuned to the same wavelength on demand using for example magnetic fields.

For illustrative purposes, consider an existing sample of diamond with N-V color centers with dipole allowed zero-phonon optical transition at 637 nm. The N-V center concentration of this diamond (on loan to us) is ~30 ppm, which corresponds to 5×10^{18} centers/cc. To achieve a high-fidelity CNOT using dipole interactions, a spatial separation of less than $\lambda/12$ between centers is assumed, since this gives an optical line splitting of 10 times its homogeneous linewidth (of 50 MHz). In a volume of $(\lambda/12)^3$ there are about 900 centers. Based on the 750 GHz inhomogeneous width, this gives an average spectral separation of 1.2 GHz (Fig. 1). Using Zeeman shifts, this frequency offset can be spanned with a variable magnetic field, tuned over a 0.6 kG range. In this example, operations would be performed on the time scale of nanoseconds. Given the spin lifetime of 0.1 msec in N-V diamond, this translates to 1000s of operations per spin lifetime.

The experiments can proceed in several stages of increasing difficulty, using previously demonstrated techniques wherever possible. In the first stage, individual N-V color centers can be observed at room temperature in a lightly doped sample, as previously demonstrated elsewhere. This can be accomplished two ways. First, the sample can be flood-illuminated with an argon laser beam at 514 nm. After passing through a holographic notch filter, the fluorescence can be imaged onto a single-photon

grade image intensifier. The output of the intensifier can in turn be imaged onto an integrating CCD camera (ICCD)(see Fig. 2a.) To detect images at the single photon level, the output of the camera can be input to a real-time frame accumulator and image processor card. This imaging system can be used to identify interesting regions of the sample and for day-to-day repeatability by insuring that the same sample location is probed each time.

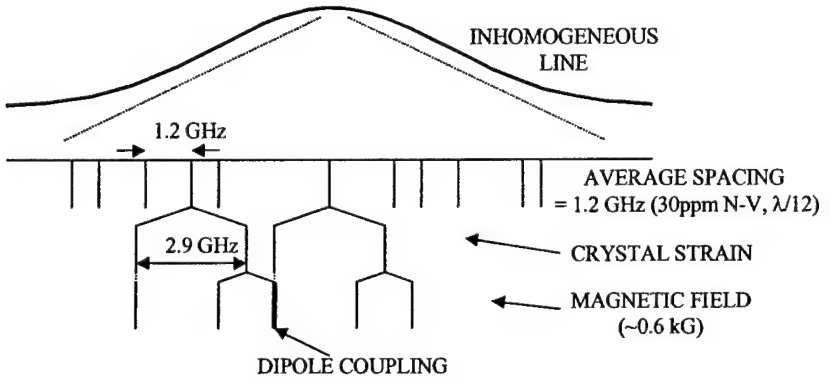

Figure 1. Illustration of spectral density of N-V color centers in diamond in a volume of $(\lambda/12)^3$ with 30 ppm concentration.

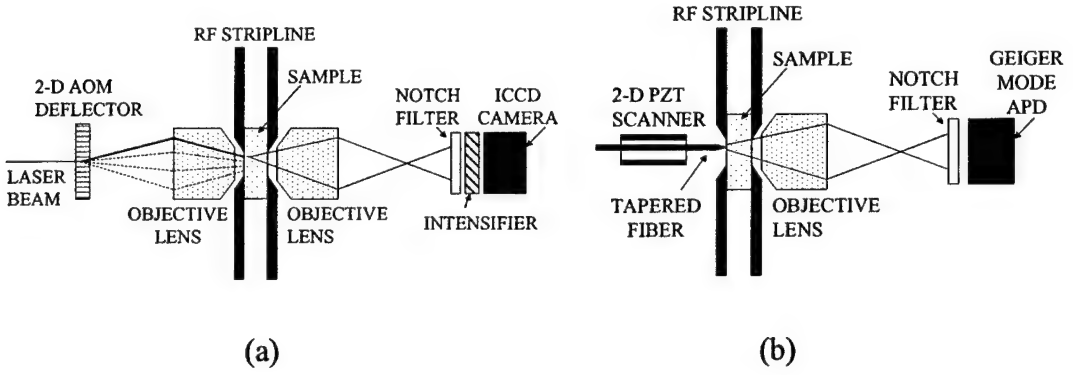

(a) (b)

Figure 2. (a) Diagram of experimental setup for probing individual color centers in a diamond sample of moderate doping concentration. Initially the scanning laser beam will be replaced by flood-illumination. The integrating video camera (ICCD) will be followed by a frame accumulator. (b) Experimental setup of near-field excitation of coupled dipoles. To perform logic operations better, the video camera will eventually be replaced by a higher quantum efficiency avalanche photodetector (APD).

Next, the flood-illumination can be replaced by a focused argon laser spot that is steered using a 2-D acousto-optic angle scanner (AOM), where the angle is converted into position by a microscope objective lens. This scanner is capable of slow raster scans to verify the local spatial distribution of color centers, but can primarily be configured to steer to a particular angle, so as to illuminate a single color center. Fluorescent light from this color center can then be collected and imaged onto the photon-counting camera

system. Once this system has been tested at room temperature, the experiment can be repeated at liquid helium temperature by inserting the sample, with objective lenses, into a cryostat.

After the first low temperature test is complete, the diamond sample can be replaced by one with a higher N-V concentration such that there will be 100-1000 color centers within a focused laser spot. In this case the color centers can only be resolved by using both spatial and spectral techniques and the argon laser illumination will be replaced by a dye laser tuned within the zero phonon line. As before, a holographic notch filter can be used to reject scattered laser light and detection will be accomplished using phonon sideband fluorescence. Alternatively, backscattered fluorescence can be used for detection, wherein the laser-focusing objective also collects the florescence, which is then diverted by a beamsplitter onto the photon-counting camera system using auxiliary imaging optics.

Within a laser beam focal volume on the order of λ^3, most atoms with similar spectral response will be too far apart to experience large dipole-dipole interactions. However, one in 100 should have interactions large enough to split an optical absorption line by more than its width. This ratio can be improved by finding atoms whose fluorescence intensity falls off at the same rate when the focused laser spot is moved slightly in the x or y directions. The image subtraction capability available in the image accumulator/processing system can facilitate this. Once a suitable pair of color centers has been identified, a CNOT experiment can then be performed, noting that diamond N-V color centers are exceptionally stable and are expected to remain unchanged in properties, even with repeated laser excitation. Initially, a quasi cw experiment can be performed wherein it is verified that the splitting of an absorption line can be turned on or off by changing only the ground state which the control atom occupies. This will demonstrate that a CNOT is possible. Next a pulsed version of a CNOT can be implemented. It is anticipated that this pulsed experiment will require higher fluorescence detection efficiency. At this point, the single-photon imaging system can be replaced by a single-photon counter, based on an avalanche photodiode (APD). The APD has more than an order of magnitude greater photon efficiency at wavelengths above 630 nm. (see Fig. 2b).

To couple more than one pair of color centers, a higher N-V center concentration is needed. In this case, there will be more color centers within a focused laser spot than it will be possible to resolve spectrally. The laser focusing lens will have to be replaced by a near field imaging system consisting of a tapered fiber optic tip with a tip diameter on the order of $\lambda/10$. Typically these tips are made by pulling a length of silica fiber on a modified commercial pipette puller. As shown in Fig. 2b, the x-y-z position of this tip can be controlled by a piezoelectric transducer (PZT), having a cylindrical shape and a 4-segment electrode. In this case fluorescence detection must be accomplished with an objective lens on the opposite side of the sample.

The goal of these experiments is to use previously demonstrated techniques to perform single color center spectroscopy of N-V diamond in the near dipole-dipole coupling regime. Once this has been achieved, the feasibility of a CNOT can be demonstrated spectroscopically by adjusting initial ground state populations and applying the appropriate pulses.

3.6 Design of a Photonic Band Gap Based Cavity in an NV-Diamond Substrate

One of the most important criteria in making a quantum computer is that one must be able to realize a CNOT operation between two nearest-neighbor qubits. We have identified in explicit detail two different methods for achieving this objective in NV-diamond. The first method, applicable to high-density of color centers, uses the direct optical dipole-dipole coupling between two qubits that are very close to each other spatially, and can be turned into spectral neighbors via applying a magnetic field. This method is somewhat limited in the number of bits that can be coupled. The second method, applicable to low-density of color centers, uses a high-finesse optical cavity, resonant with a transition common to both bits, to enhance the optical dipole-dipole coupling. The number of qubits that can be realized this way can in principle be as high as 10^5. While such a high number would be difficult to realize in practice, it should be possible to realize a more modest number (~300) qubits without much trouble.

For efficient cavity-induced coupling, a high value of Q ($2X10^5$) is achievable using the so-called super-mirrors, manufactured by the Research Electro Optics, Inc., of Boulder, CO. However, this number is virtually impossible to achieve in the presence of NV-diamond between the cavity mirrors. Even a small amount of loss resulting, for example, from Fresnel reflections will reduce the Q by orders of magnitude. As such, the idea of using bulk super mirrors of this type is essentially impracticable.

In principle, one could overcome this problem by making the cavity volume small enough so that the ratio of the vacuum rabi-frequency to the cavity decay rate becomes favorable. However, in order to allow unimpeded access of the control-lasers, the separation between the mirror surfaces has to be at least 5 to 10 times the wavelength of interest (λ~637 nm). Furthermore, the machining process used to taper the tips of the mirrors constraints the lateral dimensions to at least a 100 μm. Under these constraints, it is virtually impossible to make the vacuum rabi frequency stronger than the anticipated poor cavity decay rate in the presence of reflection losses from the surfaces of the embedded crystal. A photonic band gap (PBG) cavity holds the best promise to overcome this constraint[1]. The small mode volume of the PBG cavities (on the order of λ^3) implies that the coupling of cavity photons to atoms in the cavity will be enhanced by three or more orders of magnitude over conventional bulk-mirror based cavity couplings. As a result, the number of operations that can be performed before decoherence will be higher by nearly the same ratio.

Another key feature of this approach is that a large number of PBG cavities can be realized on the same substrate. Intercoupled qubits inside each cavity will constitute a single QC. As such, the whole substrate will contain many QC's that can be operated simultaneously. As mentioned above, such a structure is ideally suited for type II quantum computing on a large scale.

We have developed a concrete design to realize a PBG cavity in NV-Diamond in order to demonstrate the feasibility of a QC array where (i) each QC will have a large number of coupled qubits, (ii) the total number of QC's can be very high, as suited for type II quantum computing, and (iii) many operations can be performed before

decoherence. We will use a variation of the method demonstrated recently by Masuda et al. to realize the PBG structure necessary for quantum computing. First, a custom-mask will be made using lithographic techniques. The pattern on the mask will then be transferred to an NV-diamond crystal surface using chemical etching. The resulting structure will consist of a two dimensional periodic array of holes, with periodicity of the order of the wavelength (λ~637 nm) of interest. The symmetry will be broken by replacing a 3X3 grid of these holes with a hole of a larger diameter. The area around this anomalous hole will constitute the cavity, with a mode volume of the order of a few λ^3. Many such cavities will be formed on the same substrate. An important element of our quantum computing protocol requires that the cavity resonance frequency be tunable rapidly, in order to move the coupling process from one set of spectral neighbors to a different one. In order to achieve this capability, the anomalous hole in the center of the cavity will be filled with a non-linear glass. The cavity frequency then can be tuned simply by applying a suitably intense laser beam, which can be done very rapidly.

The basic design we have developed for realizing PBG cavities in diamond is illustrated in figure 1. Up to 10^4 cavities will be formed on the same substrate, as illustrated in figure 3. The structure shown in figure 1 consists essentially of a thin film of diamond, sandwitched between two glass surfaces of lower index for the vertical confinement of the cavity mode. The PBG configuration is produced by the presence of a periodic array of holes of the same diameter, with a larger diameter hole replacing a 3X3 grid of this pattern. The anticipated mode pattern is illustrated schematically by the red circle. The color centers under the red circle will be the qubits, coupling to one another through the cavity photons.

The first step will be to perform finite-element type simulations of Maxwell's equations in order to optimize the parameters of this design: the thickness of the diamond layer, the diameter of the periodic holes, and the diameter of the anomalous hole. The primary criterion optimization is to maximize the Q of the cavity. One has to also calculate the exact mode pattern, and determine the value of the vacuum rabi frequency.

Figure 2 illustrates schematically the multistage layering and etching process to be used to realize the PBG cavity array in NV-diamond. These steps can be implemented using the facilities of the Materials Technologies Laboratory at MIT. The starting point is a thick SiO_2 wafer, with an area close to 1 cm^2, available commercially. Microwave enhanced chemical vapor deposition (CVD) will be used to deposit a synthetic diamond film on this substrate. Nitrogen vacancy color centers will then be created using ion implantation, followed by annealing at 750 C. This will be followed by the growth of five additional thin layers on the diamond film: SiO_2, alumina, polyimide, SiO_2, and PMMA, as shown here.

The desired pattern of holes may be generated using a CAD program. This pattern will then be transferred to the PMMA substrate using E-beam lithography. A series of etching steps, with different ions (as shown on the right of the diagram in figure 2) will be used to transfer this pattern to the diamond. The choice of reactive ions is dictated by the need to avoid etching of the masks. For example, alumina is resistant to the oxygen plasma used for etching the holes in diamond. Finally, the holes in diamond will be filled with a non-linear optic material. Excess material above the top SiO_2 layer will be removed chemically, leaving the structure shown in fig. 1.

Once we develop the PBG cavities in NV-diamond, we will be in a position to realize the scheme of coupling two qubits via a cavity photon, in order to demonstrate a CNOT gate. In order to achieve this goal, we will first determine the transition frequency, the vacuum rabi frequency, and the Q of one of the cavities. This will be done as follows. A single color center at the cavity location will be optically pumped into one of its hyperfine states. A laser π-pulse will be applied along one of the legs of the Λ transition. The population in the other hyperfine state will then be measured by applying a laser along the other leg of the Λ transition. This process will be repeated many times while the cavity is tuned by varying the intensity of the auxiliary laser beam applied to modulate the index of the non-linear glass in the holes. The signal observed will be maximum when the cavity is tuned to the second leg of the Λ transition. The amplitude of this resonant peak can be used to determine the strength of the cavity field, i.e., the vacuum rabi-frequency. The width of the resonance will reveal the Q of the cavity. Once the cavity is characterized, we will identify and isolate two color centers that are spectral neighbors. The steps described in previous reports for demonstrating a CNOT gate will then be implemented.

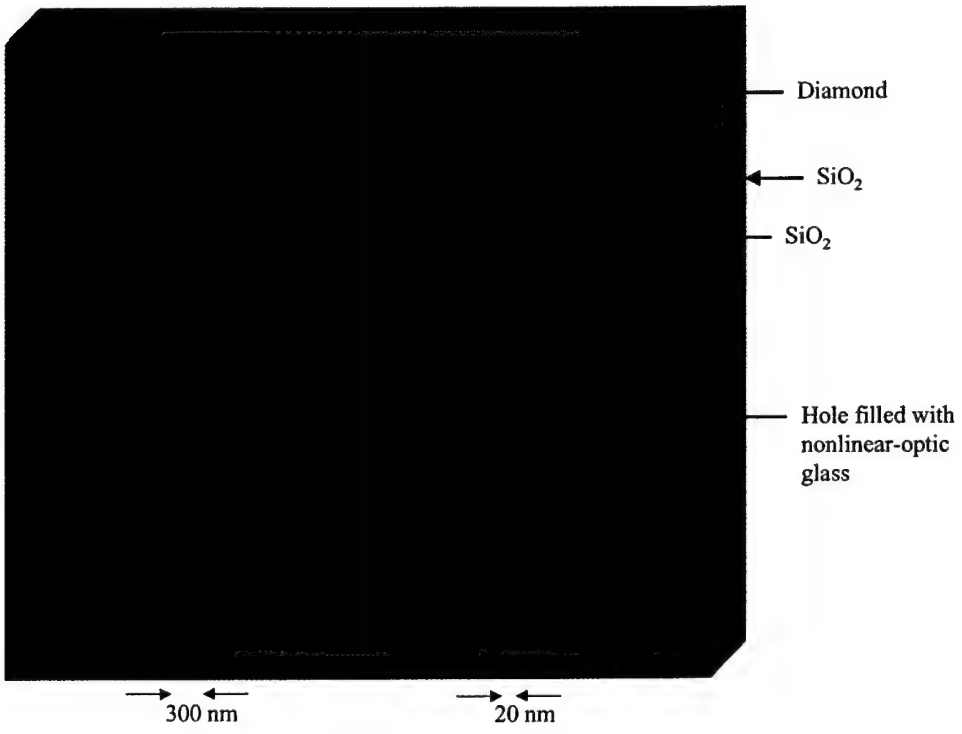

[A]

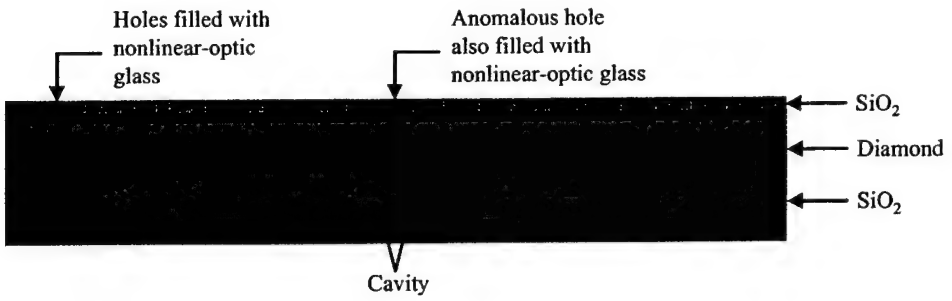

[B]

Figure 1. *Schematic illustration of the proposed PBG cavity structure in NV-Diamond. (a) Top view (b) Cross-sectional view. This will be one of many (up to 10^4) cavities formed on the same substrate, as illustrated in figure 3. The pattern shown here can be produced using the multi-stage process summarized in figure 2. The finished structure shown here consists essentially of a thin film of diamond, sandwitched between two glass surfaces of lower index for the vertical confinement of the cavity mode. The PBG configuration is produced by the presence of a periodic array of holes of the same diameter, with a larger diameter hole replacing a 3X3 grid of this pattern. The anticipated mode pattern is illustrated schematically by the red circle; of course, the real pattern will have some asymmetry. The color centers under the red circle will be the qubits, coupling to one another through the cavity photons.*

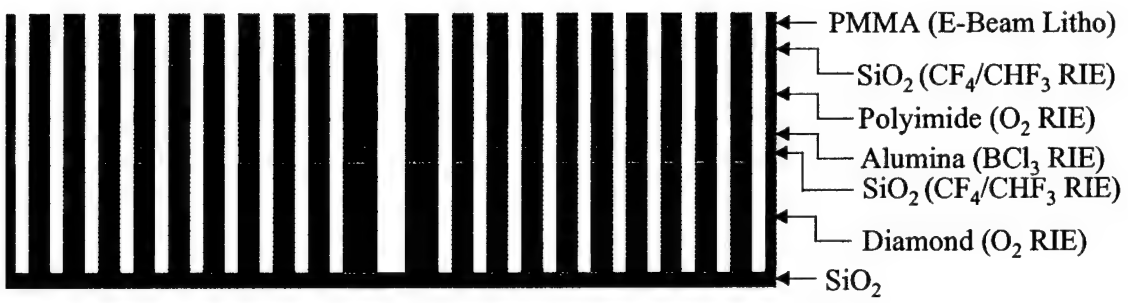

Figure 2. Schematic illustration of the proposed multistage layering and etching process, to be implemented using the facilities of the materials technologies laboratory at MIT. The starting point is a thick SiO_2 wafer, with an area close to 1 cm^2, available commercially. Microwave enhanced chemical vapor deposition (CVD) will be used to deposit a synthetic diamond film on this substrate. Nitrogen vacancy color centers will then be created using ion implantation, followed by annealing at 750 C. This will be followed by the growth of five additional thin layers on the diamond film: SiO_2, alumina, polyimide, SiO_2, and PMMA, as shown here. The desired pattern of holes will be generated using a CAD program. This pattern will then be transferred to the PMMA substrate using E-beam lithography. A series of etching steps, with different ions (as shown on the right of the diagram) will be used to transfer this pattern to the diamond. The resulting holes will then be filled with a non-linear optic material. Excess material above the top SiO_2 layer will be removed chemically, leaving the desired structure.

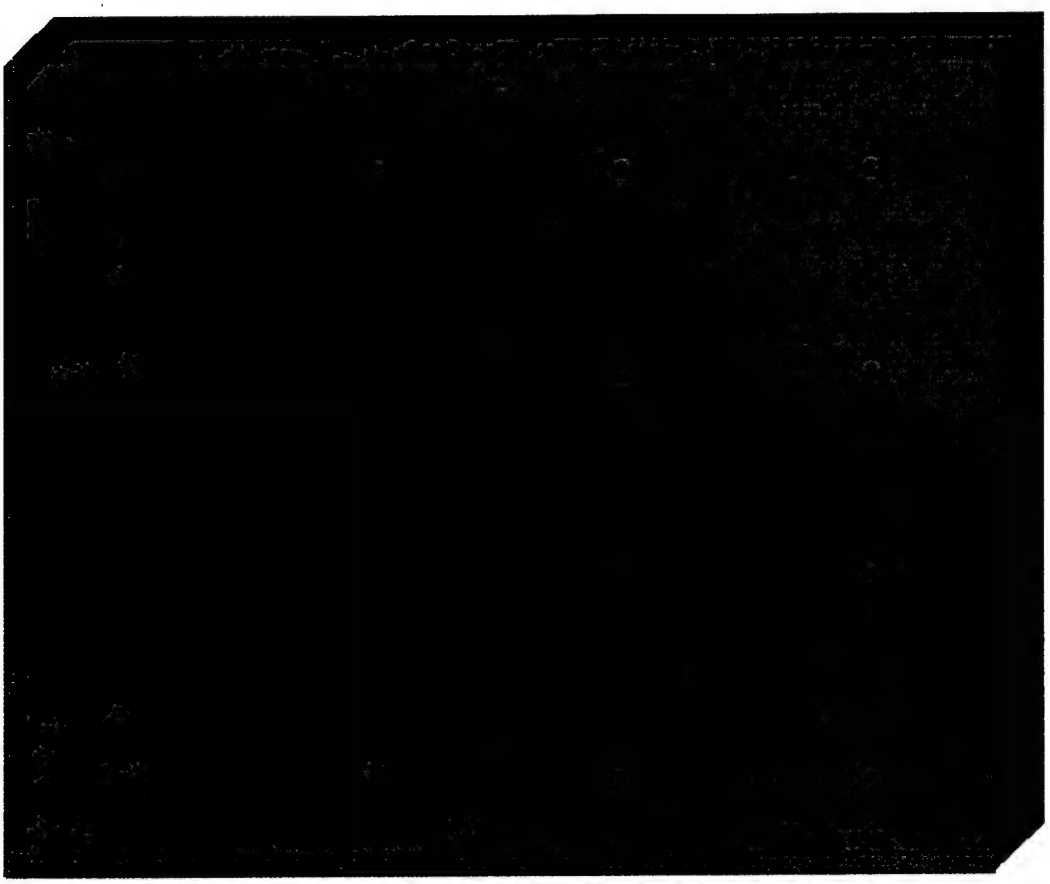

Figure 3: *Schematic view of the array of PBG cavities for Type II quantum computing. Here, each cavity represents a single QC. The total number of QC's on a single chip with an area of 1 cm^2 can be easily as high as 10^4. A computer-controlled, analog spatial-light modulator (available in sizes as large as 1000X1000 elements) can be used to control the intensities of the laser beams for each QC separately. Of course, such independent controls are necessary only for general purpose quantum computing. For type II quantum computing, on the other hand, all the QC's can in principle be operated in an identical manner, thereby simplifying the programming task enormously.*

3.7 High-Resolution Mapping of NV-Color Centers

As mentioned above, one of the conditions for realizing a CNOT gate is the ability to isolate and detect single color centers. Techniques for spectral isolation via shelving has been described in detail previously. We have made recent experimental progress towards spatial isolation and detection. Briefly, we used a diamond sample with color centers on its surface. Figure 71shows the basic geometry used. Two acousto-optic modulators were used to scan a laser beam in two dimensions, while remaining focused on the surface of the sample. The fluorescence generated was collected with a microscope objective, filtered, and then detected using a Geiger mode avalanche photo diode (APD). The scanning process was controlled by a DAC card installed in a computer, which also recorded the two dimensional image resulting from the raster scan. A typical scan obtained this way is shown in figure 2. The deep purple line shows one of the lines of color centers. An isolated cluster of color centers is seen about 10 μm away. The next step is to use the optical shelving technique to reduce the active number of centers to unity in such a cluster.

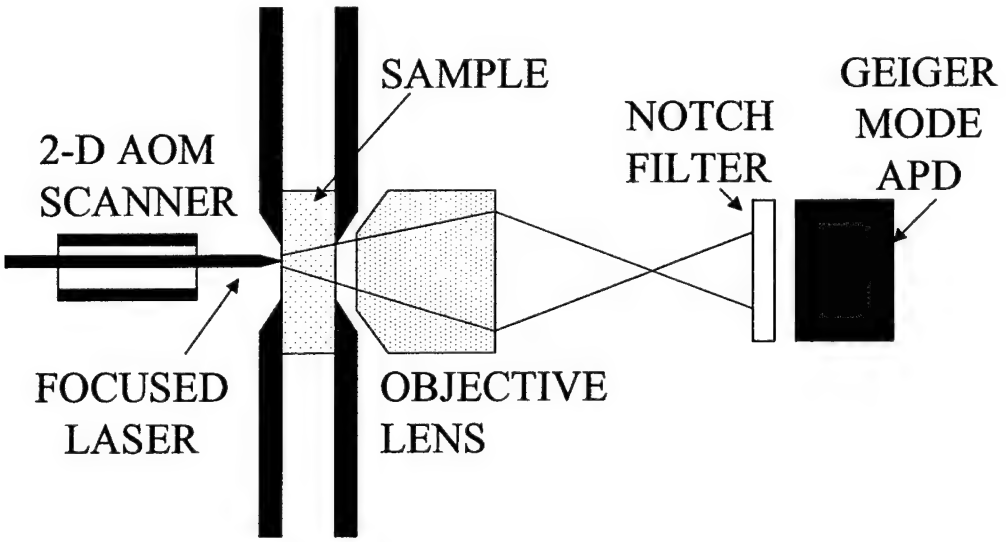

Figure 1. Schematic illustration of the configuration used for detecting small clusters of color centers on the surface of a diamond crystal. When combined with spectral shelving, this technique will enable the detection of single color centers.

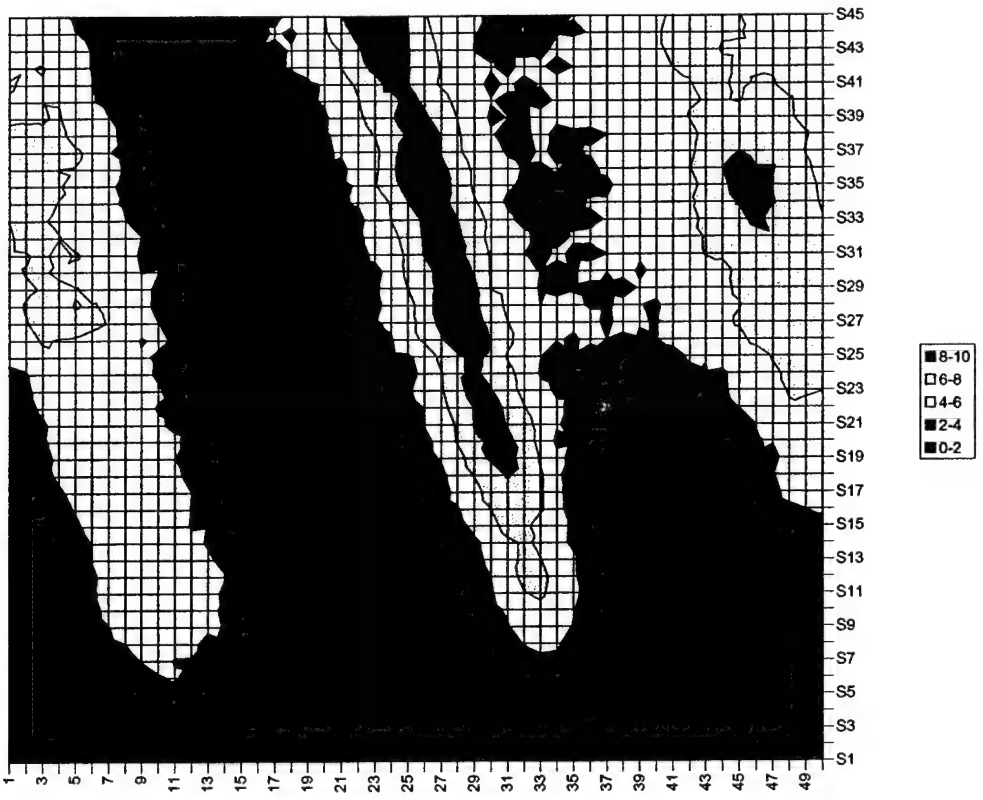

Figure 2. A typical raster scan of the surface of a diamond crystal with color centers created on its surface, using the apparatus of figure 1. The deep purple line shows one of the lines of color centers. An isolated cluster of color centers is seen about 10 μm away. The next step is to use the optical shelving technique to reduce the active number of centers to unity in such a cluster.

3.8 Slowing and Storage of Light Pulses in Pr:YSO: A quantum memory for photons

Since the first observation of ultraslow light, there has been substantial interest in its potential applications. For example, it was proposed that slowing the group velocity of a laser pulse down to the speed of sound in a material can produce strong coupling between acoustic waves and the electromagnetic field. The resultant giant nonlinearity obtained by this method might be utilized for efficient multi-wave mixing and quantum nondemolition measurements, as well as for novel acousto-optical devices. A carefully controlled, slow group velocity of light might even allow a very efficient nonlinear interaction between laser pulses of extremely low (down to a single photon) energy. These effects can be used to create quantum entanglement between single photons without an ultrahigh finesse cavity and therefore are of great interest for quantum information processing. Slow light is also of interest because it serves as a useful metric to compare the relative merits of dissimilar nonlinear optical interactions. This is especially important for applications that make use of large optical dispersive properties of EIT for the detection of small phase shifts, such as in very sensitive magnetometers.

Initially, ultraslow light was observed in an ultra cold atomic vapor using the sharp dispersion caused by electromagnetically induced transparency (EIT). EIT, which is related to coherent population trapping, uses an intense electromagnetic field is used to modify the absorption coefficient and refractive index seen by a weak probe so that an optically dense media can be made nearly transparent to light at its resonance frequency. In addition, the sharp dispersion of EIT leads to a slow group velocity for the propagation of light, tuned to the frequency of the transparency peak. At first it was believed that only a material with a small inhomogeneous broadening could be used to achieve ultraslow light, but subsequent experiments employing a hot vapors were soon shown to work better than expected. Still, for a number of applications, the need to compensate for Doppler shifts in a hot vapor by using nearly co-propagating laser beams is inconvenient. Finally, for potential technological device applications of ultraslow light, there is no substitute for solids.

Recently, we reported near 100% efficient EIT in a Pr^{3+} doped Y_2SiO_5 (Pr:YSO) crystal wherein transparency of probe field was demonstrated at line center in an optically thick sample. At low temperatures, this "dark resonance" has a width on the order of 10's kHz. This potentially makes it suitable for the direct measurement of ultra long optical group delays because the group delay time for a pulse that propagates one attenuation length is approximately given by to the inverse width of the EIT peak assuming 100% efficient EIT. We would like to note that Pr:YSO and many rare-earth doped crystals have properties similar to both hot and cold atomic vapors. In particular, both Pr:YSO and ultra cold vapors, have the advantage that there is no motional diffusion of atoms, whereas Pr:YSO and hot vapors have the common advantage that the light speed can be slowed to well below the sound speed in the medium.

Our crystal was supplied by Scientific Materials, Inc. and consisted of 0.05 at% Pr doped YSO in which Pr^{3+} substitutes Y^{3+}. The crystal had a thickness of 3 mm in the light

propagation direction. To generate the EIT peak, we used the $^3H_4 \rightarrow {}^1D_2$ optical transition with a central frequency of 605.7 nm. The relevant energy level diagram is presented in Figure 1. Here, the coupling and the probe fields, with frequencies ω_C and ω_P respectively, create a coherence the between ground states $^3H_4$ ($\pm 3/2 \leftrightarrow \pm 5/2$), while the repump field with frequency ω_R partially refills the spectral holes burned by the coupling and the probe fields. This partial refilling or anti-hole also provides a narrow effective optical inhomoheneous linewidth for the Raman transitions. The experimental arrangement is similar to that used in Ref. 14. This time, we used a COHERENT 899-21 single mode ring dye laser pumped by an INNOVA 300C argon laser. The dye laser was continuos wave with a laser jitter measured to be about 0.5 MHz. All the laser fields shown in Figure 1 were derived from the dye laser output using acousto-optic frequency shifters. This greatly relaxes dye laser frequency stability requirements since the resonant Raman interaction is insensitive to correlated laser jitter. To match Figure 1, the coupling, repump, and probe beams were downshifted from the original laser frequency by 288.3, 311.0, and 298.5 MHz respectively. To generate the probe beam absorption spectra, the probe frequency was scanned around the 10.2 MHz Raman transition frequency while the frequencies of the coupling and the repump beams were held fixed. A set of compensating galvos was used to correct for the optical alignment changes that arise when the acousto-optic modulators are tuned. The intersection angle of the coupling and probe beams at the crystal was about 4° in the plane of the optical table. The intersection angle of the repump beam was also 4° but out of the plane of the optical table. This geometrical arrangement allowed us to reduce the effects of scattered light from the coupling and the repump beams. To further increase the signal to noise ratio, the probe beam was modulated and the transmitted signal was detected by standard phase-sensitive detection techniques. All laser beams were linearly polarized and focused into the crystal by a 150 mm focal length lens, producing a spot with a diameter of about 100 □m. The beams were polarized in a common direction that could be rotated by a half-wave plate to maximize absorption for a given orientation of the crystal. During the experiment, the sample was maintained at a temperature of 5.5 K inside a helium flow JANIS cryostat.

The dye laser was locked near the center of the inhomogeneously broadened absorption line at 605.7 nm. The intensities of the probe and repump fields were held fixed during the experiment at 0.1 and 1.6 W/cm^2, respectively. The background absorption was determined by the anti-hole, which was created by the repump beam, and superimposed on the much broader, saturated hole burned by the pump beam. The width of anti-hole was found to be about 0.5 MHz and was defined by the dye laser frequency jitter. The width of the saturated hole was not determined due to the limited 50 MHz bandwidth of the acousto-optic modulators, but appeared to be much larger than 50 MHz. Due to the limited intensity of the coupling field, the maximal transparency was found to be about 50%. Figure 2a shows a representative absorption spectrum of the probe field obtained at a coupling field intensity of 105 W/cm^2. The spectrum was recorded using phase in-sensitive lock-in detection. The measured FWHM of EIT peak was around 60 kHz for the chosen range of coupling field intensities. This is much smaller than the laser jitter of 0.5 MHz and is in agreement with the inhomogeneous linewidth of the spin transition as measured by optically detected nuclear magnetic resonance (ODNMR). The peak absorption of the probe near the center of the anti-hole line was about 90% and could be adjusted by changing the intensities of the coupling and the repump fields.

Blocking either the coupling beam or the repump beam resulted in nearly 100% transparency of the probe beam because of spectral hole burning.

The temporal retardation of the amplitude modulated probe beam tuned to the EIT peak manifests itself as a strong shift in the modulation phase that can be measured with a lock-in amplifier. Figure 2b and 2c show the absorption spectra of the probe beam for two different lock-in amplifier phases. Both spectra were recorded at a coupling beam intensity of 105 W/cm^2 and a probe beam amplitude modulation frequency of 6 kHz. Figure 2b shows the absorption spectrum recorded with the lock-in amplifier phase adjusted to suppress the broad absorption, and Figure 2c demonstrates the same absorption spectrum with the lock-in amplifier phase adjusted to suppress the EIT peak. Comparison of these two spectra clearly shows a strong dependence of the phase of modulation of the transmitted signal on the detuning from the EIT peak. To measure the group delay, the probe field was modulated with a square wave at a frequency that was varied in the range of 3 – 6 kHz. These low modulation frequencies assure that pulse spectrum is contained within the EIT peak. The group time delay was calculated based on the modulation frequency and the phase shift between the transmitted probe signal with and without the EIT-producing coupling field. Figure 3 presents the measured phase shift as a function of modulation frequency for the coupling beam intensity of 105 W/cm^2. The group delay time for this coupling beam intensity was found to be 39.6 □s from the linear fit of the data. This result is in good agreement with an estimate using the measured 62 kHz FWHM of the EIT resonance.

At low coupling beam intensities, the fraction of Pr ions that are pumped into the "dark state" increases with coupling laser power and therefore the depth of the transparency increases. This causes the group delay to increase. At higher intensities, the transparency begins to power broaden, reducing the sharpness of the dispersive feature. This reduces the observed group delay[5]. To show these saturation effects, the EIT peak width and amplitude were measured as a function of the coupling beam intensity and the results are shown in Figure 4. At intensities below 50 W/cm^2 the width of the EIT peak is defined by the inhomogeneous width of the ground state transition, and therefore it is a constant. Meanwhile the amplitude of the EIT peak increases linearly with the intensity. At high intensities above 65 W/cm^2 the width of the peak begins to increase with intensity due to power broadening, while the amplitude of the peak saturates. Comparing this data to Figure 5, which shows the group velocity and delay versus coupling beam intensity, it is apparent that there is a strong correlation between the EIT linewidths and amplitudes and the observed group velocities.

As can be seen in Figure 5, a group velocity of light as slow as 45 m/s is reached. Here, we assumed the length of an interaction zone to be 3 mm, which is the thickness of the crystal. However, due to the geometric configuration used, the interaction area where all three beams are overlapping is slightly shorter than the thickness of the crystal, so that the actual group velocities are slightly smaller than in Figure 5. In contrast to the slow light experiment in an optically dense hot vapor, the light velocity here is practically independent of the propagation distance since the intense coupling beam propagates with little attenuation. However, as shown in Figure 5 the dependence of the group velocity on the input coupling field intensity still permits fine tuning of the group delay so as to allow one to achieve phase-matched conditions in an experiment on stimulated Brillouin

scattering and/or to adjust group velocities of single photons for ultrastrong nonlinear interaction.

Additional details of this work can be found in paper #5 in our list of published papers, also attached here.

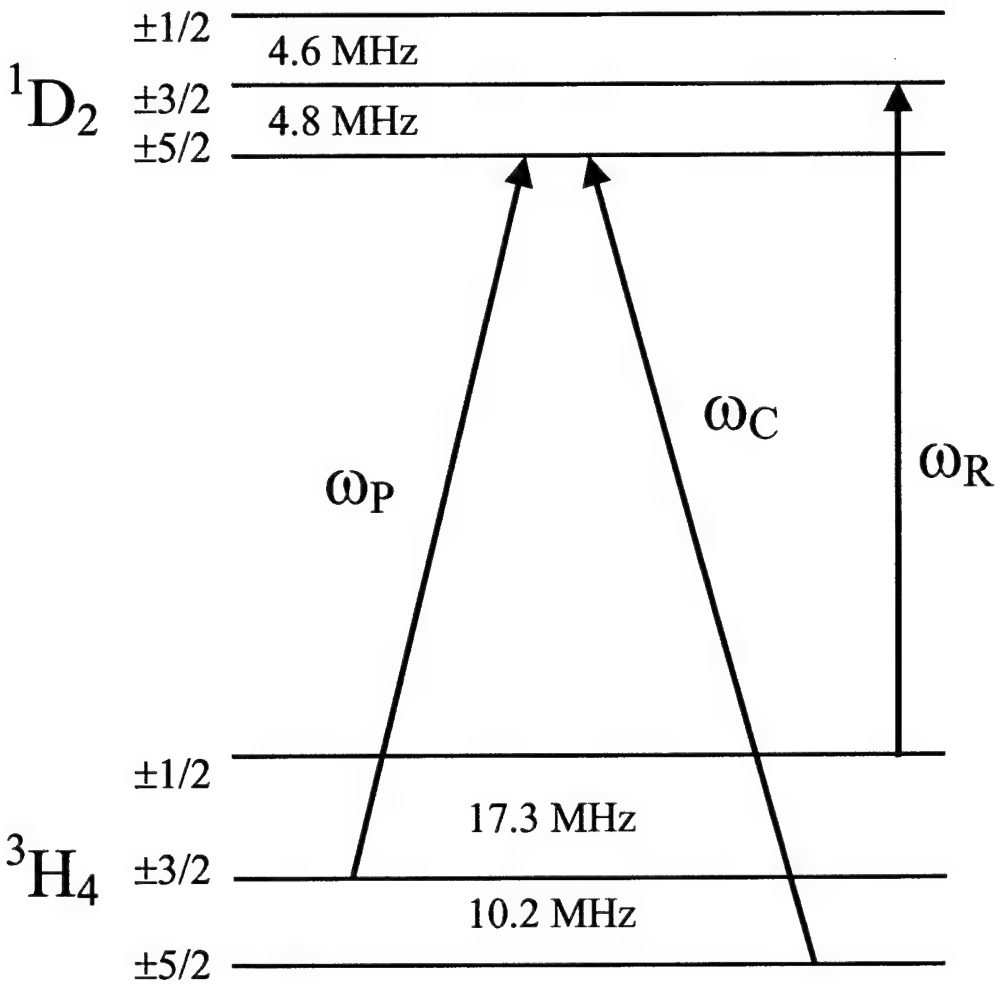

Figure 1. Energy level diagram of Pr:YSO. ω_C, ω_R, and ω_P are frequencies of the coupling, the repump, and the probe fields, respectively.

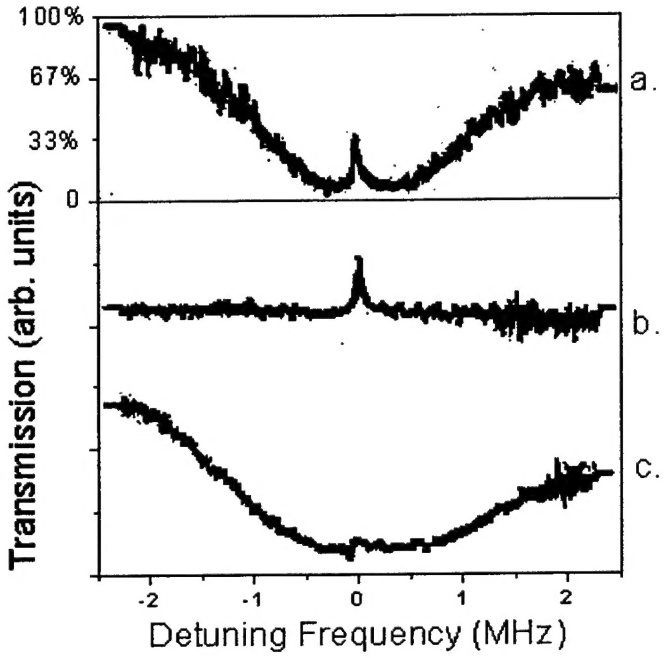

Figure 2. The absorption spectra of the probe beam at 5.5 K for a coupling field intensity of 105 W/cm^2. (a) spectrum recorded by phase in-sensitive lock-in detection; (b) spectrum recorded by phase sensitive lock-in detection with the phase adjusted to suppress the anti-hole absorption; (c) the spectrum (b) recorded with the phase adjusted to suppress the EIT peak. The modulation frequency of the probe beam was 6 kHz in for all three traces.

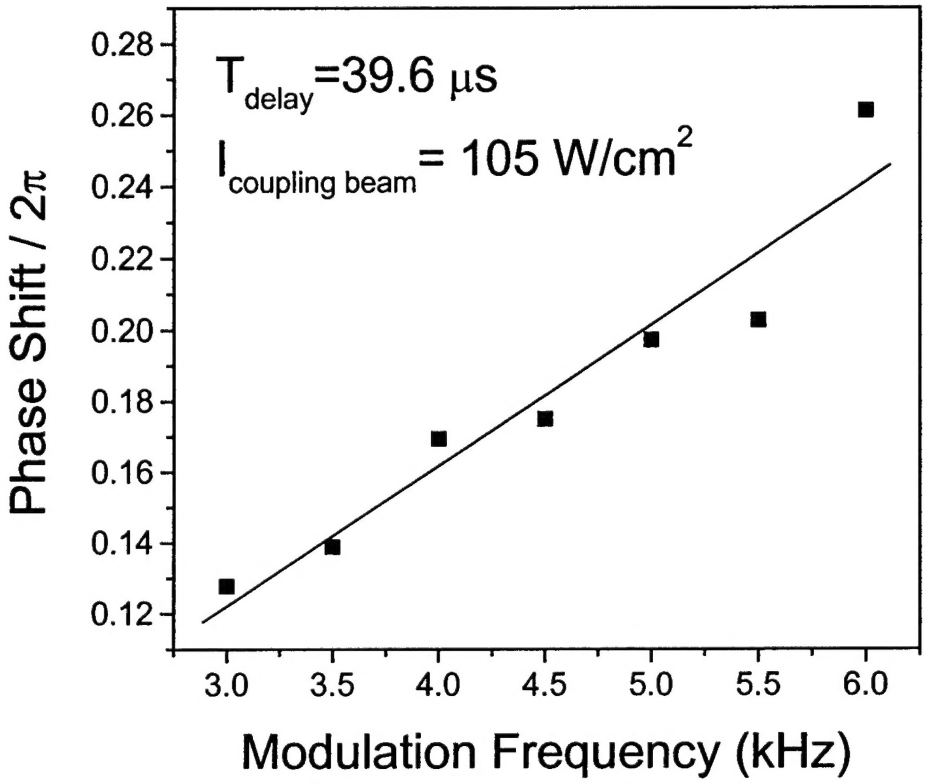

Figure 3. Phase shift between the transmitted probe signal with and without the coupling field vs. modulation frequency. The delay time was found to be 39.6 μs from the linear fit of the data.

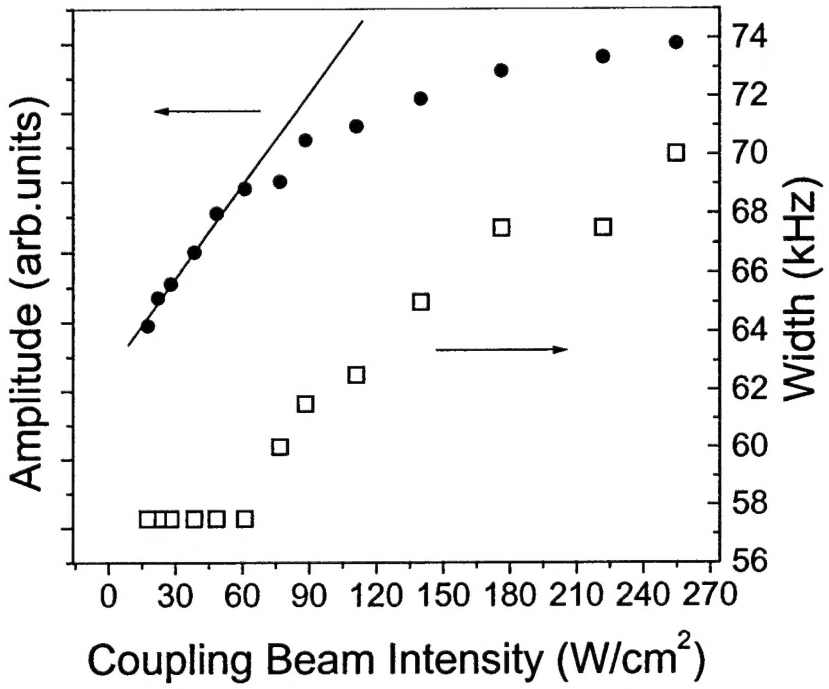

Figure 4. The EIT peak amplitude (closed squares) and width (open circles) vs. coupling beam intensity.

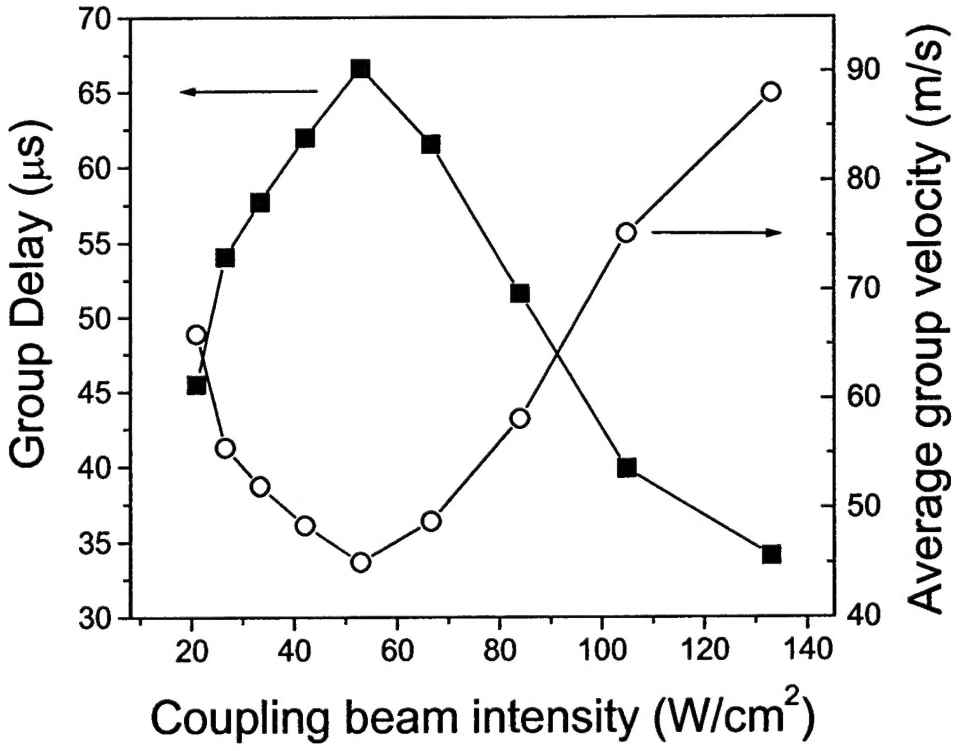

Figure 5. Measured group delays (solid squares) and deduced group velocity (open circles) vs. the intensity of the coupling field.

4. TECHNOLOGY TRANSFER:

None.